Chaos, Solitons and Fractals 199 (2025) 116669

Contents lists available at ScienceDirect

Chaos, Solitons and Fractals

journal homepage: www.elsevier.com/locate/chaos

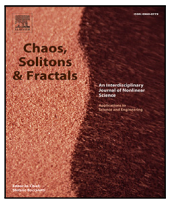

A new kind of T-point in the Lorenz system with a different bifurcation set

A. Algaba [a], F. Fernández-Sánchez [b], M. Merino [a], A.J. Rodríguez-Luis [b,*]

[a] Departamento de Matemáticas, Centro de Investigación de Física Teórica y Matemática FIMAT, Universidad de Huelva, 21071 Huelva, Spain
[b] Departamento de Matemática Aplicada II & IMUS, E.T.S. Ingeniería, Universidad de Sevilla, Camino de los Descubrimientos s/n, 41092 Sevilla, Spain

ARTICLE INFO

Keywords:
Lorenz system
T-point
Bykov cycle
Homoclinic connection
Heteroclinic connection
Degenerate T-point

ABSTRACT

In this work we find a new kind of T-point (or Bykov point) in the Lorenz system. At this codimension-two degeneracy, a heteroclinic cycle connects the origin (when it is a real saddle) and non-trivial equilibria (when they are saddle-focus). We observe that it presents a noteworthy geometric difference from the "classical" T-point, known since the 1980s in the Lorenz system. Because the dominant eigenvalue of the two-dimensional manifold at the origin changes, a variation in the direction of the corresponding heteroclinic orbit occurs near this equilibrium. Simultaneously, there is an important change in the bifurcation set, not previously found in the literature. While at the *classical* T-point the homoclinic and heteroclinic curves of non-trivial equilibria arise as half-lines in the same direction (as predicted by the well-known model of Glendinning and Sparrow), now these global bifurcation curves emerge in opposite directions. To justify this change we build a theoretical model with suitable Poincaré sections in a tubular environment of the heteroclinic cycle. Finally, by introducing a fourth parameter into the Lorenz system (a new quadratic term in its third equation), we show how the *classical* T-point can also lead to the new bifurcation set. This transition through a nongeneric situation (which occurs when the Jacobian matrix at the origin has a double eigenvalue) implies the existence of a codimension-three degenerate T-point. We find this bifurcation in the Lorenz-like system considered and illustrate how the bifurcation sets evolve by analyzing parallel parameter planes on both sides of the degeneracy.

1. Introduction

Since its appearance in the 1960s [1], the Lorenz system has been the subject of a large amount of work that has allowed to understand part of the great dynamical richness that it can present. For instance, certain aspects of the chaotic behavior the Lorenz system exhibits are considered in [2–4]. The presence of hidden chaotic attractors [5], some mechanisms of formation of periodic orbits [6], and considerations on the thermodynamic efficiency of the Lorenz equations [7] are examples of other aspects that have also received attention recently.

Given the physical significance of the Lorenz system, its three parameters are typically positive. However, in certain cases, it is also meaningful for them to take negative values. For example, Lorenz system arises in the analysis of traveling-wave solutions of the Maxwell–Bloch equations [8] and in the study of a thermosolutal convection model [9]. Thus, the study of the Hopf bifurcation (the Jacobian matrix has a pair of purely imaginary eigenvalues) [10] and the Takens–Bogdanov bifurcation (a double-zero eigenvalue with geometric multiplicity one) [11] has been carried out in their complete three-parameter space. The existence of invariant algebraic surfaces [12] and the presence of resonances in periodic orbits [13] have also been analyzed.

On the other hand, as is well known from the pioneering works of Shilnikov (see the recent survey [14] and references therein), the presence of global bifurcations (homoclinic and heteroclinic connections; remind that a homoclinic connection is bi-asymptotic to a saddle equilibrium and a heteroclinic connection joins two different saddle equilibria) can lead to complex periodic and aperiodic behavior [15, 16]. Identifying the organizing centers and the bifurcations they undergo is essential for analyzing the dynamics of parameterized systems (see, for instance, [17–19]). Regarding global bifurcations, T-point heteroclinic cycles or, more simply, T-points by abuse of notation (also referred to as Bykov cycles [20]) play a significant role.

For three-dimensional systems with at least two saddle equilibria, a T-point arises when the one-dimensional unstable manifold of one equilibrium coincides with the one-dimensional stable manifold of the other (generically, this is a codimension-two solution). Simultaneously, the two-dimensional manifolds of these equilibria intersect transversally (this is a robust, codimension-zero solution), forming a heteroclinic loop. In the Lorenz system, this codimension-two heteroclinic cycle was discovered in the 1980s [21]. In this case, it connects the origin (a real saddle equilibrium with a one-dimensional unstable manifold) and the

* Corresponding author.
E-mail address: ajrluis@us.es (A.J. Rodríguez-Luis).

https://doi.org/10.1016/j.chaos.2025.116669
Received 20 March 2025; Received in revised form 4 May 2025; Accepted 26 May 2025

nontrivial equilibria (saddle-focus equilibria with a two-dimensional unstable manifold). Remind that, in planar systems, a saddle equilibrium has two eigenvalues of different signs; in three-dimensional systems, when the three eigenvalues are real, it is named real saddle, whereas if the equilibrium has a pair of complex conjugate eigenvalues, it is called saddle-focus. This heteroclinic cycle occurs at a point in the parameter plane, from which three global bifurcation curves emerge [22]. These curves correspond to homoclinic connections to the origin (it has spiral shape) as well as homoclinic and heteroclinic connections of the nontrivial equilibria (both curves arise as half-lines in the same direction). Throughout this paper, we will refer to it as the *classical* T-point.

The existence of T-points has been demonstrated in many systems from different areas. Without claiming to be exhaustive, we list a few of them: Shimizu–Morioka model [23], Chua's equation [24,25], a low-order model of magnetoconvection [26,27], a laser model [28], a modified van der Pol–Duffing electronic oscillator [29,30], and a model of the oxidation on platinum surfaces [31,32]. Interesting results have also been found on the relationship between spiral structures and T points (see, for instance, [33,34]). The existence of possible degeneracies at T-points has also been discussed in the literature. For example, a T-point-Hopf arises when one of the equilibria experiences a Hopf bifurcation [35–37]. On the other hand, valuable results on the dynamics near T-points appear, for instance, in [38–40].

In this work, we identify a new kind of T-point heteroclinic cycle in the Lorenz system with a distinct geometric structure. Additionally, we detect that the arrangement of the global bifurcation curves emerging from it is different from that appearing in the *classical* T-point. Specifically, the two curves of global connections of the nontrivial equilibria emerge as half-lines but in opposite directions. This indicates the existence of a degenerate T-point (codimension-three bifurcation), due to the presence of a double eigenvalue in the Jacobian matrix at the origin (a transition through a nongeneric situation which implies a change in the bifurcation set, not previously found in the literature). We also find this degeneracy in a Lorenz-like system that we analyze.

This paper is organized as follows. In Section 2, we consider the Lorenz system and find, in a region of the parameter space, a new T-point. After comparing it with the *classical* T-point we point out two important differences in its geometry. In addition, as mentioned above, a fundamental change appears in the way in which the homoclinic and heteroclinic curves of nontrivial equilibria arise, since, although they are still half-lines, they appear in opposite directions. In Section 3, we propose a theoretical model using Poincaré sections (suitably modifying the Glendinning and Sparrow model [22]), which allows us to satisfactorily justify the new bifurcation set. In this way, we demonstrate that the existence of a double eigenvalue in the Jacobian matrix at the origin generates a codimension-three T-point. In Section 4, we introduce a fourth parameter in the Lorenz system (a new quadratic term in its third equation). This helps us to find regions in the parameter space in which the *classical* T-point evolves and gives rise to the new bifurcation set. In this way, we find a degenerate T-point in the Lorenz-like system considered. Finally, a Conclusions section is included.

2. Detection of a new T-point

The Lorenz system is given by (see [1])

$$\begin{cases} \dot{x} = \sigma(y - x), \\ \dot{y} = \rho x - y - xz, \\ \dot{z} = -bz + xy, \end{cases} \tag{1}$$

where σ, ρ and b are real parameters (note that if $\sigma = 0$ the system becomes linear and if $b = 0$ all the points in the z-axis are non-isolated equilibria). The Lorenz equations are invariant under the change $(x, y, z) \to (-x, -y, z)$. It has up to three equilibria namely, the origin, $E_0 = (0, 0, 0)$, and when $b(\rho - 1) > 0$, two symmetric nontrivial equilibria $E_\pm = (\pm\sqrt{b(\rho-1)}, \pm\sqrt{b(\rho-1)}, \rho - 1)$.

As the eigenvalues of the Jacobian matrix at the origin are going to be important in our study, we write their expressions

$$\lambda_{1,2} = \frac{-(1+\sigma) \mp \sqrt{(1+\sigma)^2 + 4\sigma(\rho-1)}}{2}, \qquad \lambda_3 = -b. \tag{2}$$

It is easy to check that the eigenspaces of λ_1 and λ_2 are both located in the plane $z = 0$ whereas the eigenspace of λ_3 is the z-axis.

Since in this section we are going to find a new T-point in the Lorenz system, it is convenient to start by recalling some results about the first T-point detected (the *classical* T-point). After identifying a T-point numerically in the Lorenz system [21], Glendinning and Sparrow [22] presented a theoretical analysis demonstrating that the unfolding of this codimension-two bifurcation involves three primary curves (see [22, Figs. 2 and 3], [3, Fig. 1]). These include a spiraling curve **Ho** associated with two simultaneous homoclinic connections of the origin (due to symmetry), a half-line **Hnt** representing two simultaneous homoclinic connections of the nontrivial equilibria, and another half-line **He** corresponding to a pair of symmetric heteroclinic orbits linking the nontrivial equilibria. They demonstrated that, to first order, the curves **Hnt** and **He** emerge in the same direction.

In Fig. 1(a), for $\rho = 50$, we draw the projection onto the x-z plane of the *classical* T-point heteroclinic cycle, which exists in Lorenz system when $b \approx 4.76314$, $\sigma \approx 18.2482$. In this region of the parameter space the origin is a real saddle (with $\lambda_1 < \lambda_3 < 0 < \lambda_2$, according to Eq. (2)) and the nontrivial equilibria are saddle-focus (with positive real part of the complex eigenvalues). We observe that the heteroclinic orbit corresponding to the intersection of the two-dimensional manifolds (in red) reaches the origin tangentially to the z-axis. This can be explained by examining the eigenvalues of the Jacobian matrix at the origin, which, for these parameter values, are (see Eq. (2)): $\lambda_1 \approx -41.04$, $\lambda_2 \approx 21.79$, and $\lambda_3 \approx -4.76$. Since $|\lambda_3|$ (whose eigenvector coincides with the z-axis) is smaller than $|\lambda_1|$ (whose eigenvector is located in the plane $z = 0$), the dominant direction near the origin is that of the z-axis (and this is, therefore, the generic entry direction). This fact is very evident since $\lambda_1/\lambda_3 \approx 8.62$.

In Fig. 1(b), we show a partial bifurcation set in the (b, σ)-plane, in a neighborhood of the *classical* T-point. According to [22], **Ho** emerges spiraling and the curves **Hnt** and **He** are half-lines arising in the same direction. Note that **Hnt** and **He** are so close that they are not distinguishable. More details of this bifurcation set can be found in [37].

In what follows, to find the new T-point in the Lorenz system, we will focus on a region of the parameter space where we know that homoclinic connections of the origin exist. For this, we rely on analytical and numerical results concerning Hopf and Takens–Bogdanov bifurcations in the Lorenz system (see [10,11]). For example, we know that when $\rho = 1$, $\sigma = -1$ and $b < 0$, the origin undergoes a homoclinic-type Takens–Bogdanov bifurcation. In the considered region, since $\rho < 1$, $b < 0$, $\sigma < 0$, according to (2), the origin is a real saddle with $\lambda_1 < 0 < \lambda_2, \lambda_3$. All numerical results will be obtained with the help of the continuation code AUTO [41]. Keep in mind that, for the sake of simplifying the notation throughout this paper, we will use the same symbol to label both the global connections (which, due to symmetry, actually come in pairs) and the global bifurcations, despite them being distinct objects.

Since in [11, Fig. 10] the case $b = -1.6$ was studied, we now fix another value of b closer to $b = -2$, for which a degenerate homoclinic-type Takens–Bogdanov bifurcation of infinite codimension occurs. Thus, we begin by obtaining a partial bifurcation set for $b = -1.95$. To do this, we take $\rho = -0.05$, $\sigma = -0.025$, and continue the non-trivial equilibrium E_+, moving ρ. A Hopf bifurcation **h** is detected when $\rho \approx -0.0277027$. The bifurcation diagram of the repulsive periodic orbit arising from **h** is drawn in Fig. 2(a). As can be seen in this figure, this periodic orbit experiences two period-doubling bifurcations ($\mathbf{pd_1}$ for $\rho \approx -0.0210674$ and $\mathbf{pd_2}$ for $\rho \approx 0.0715419$) and a saddle–node bifurcation **sn** when $\rho \approx 0.0715420$. The saddle periodic orbit that arises

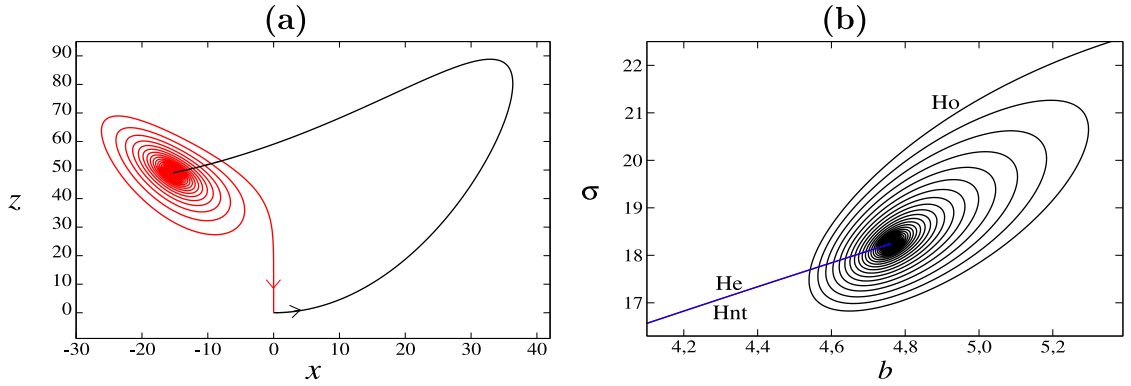

Fig. 1. For $\rho = 50$: (a) Projection onto the x-z plane of the T-point heteroclinic cycle in Lorenz system, which exists when $b \approx 4.76314$, $\sigma \approx 18.2482$. (b) Partial bifurcation set in the (b, σ)-plane, in a neighborhood of the T-point. Three curves of global connections emerge, namely, **Ho** (spiraling curve of homoclinic orbits to the origin), **Hnt** (of homoclinic connections of the nontrivial equilibria) and **He** (of heteroclinic connections between the nontrivial equilibria). Note that the curves **Hnt** and **He** are so close that they are not distinguishable.

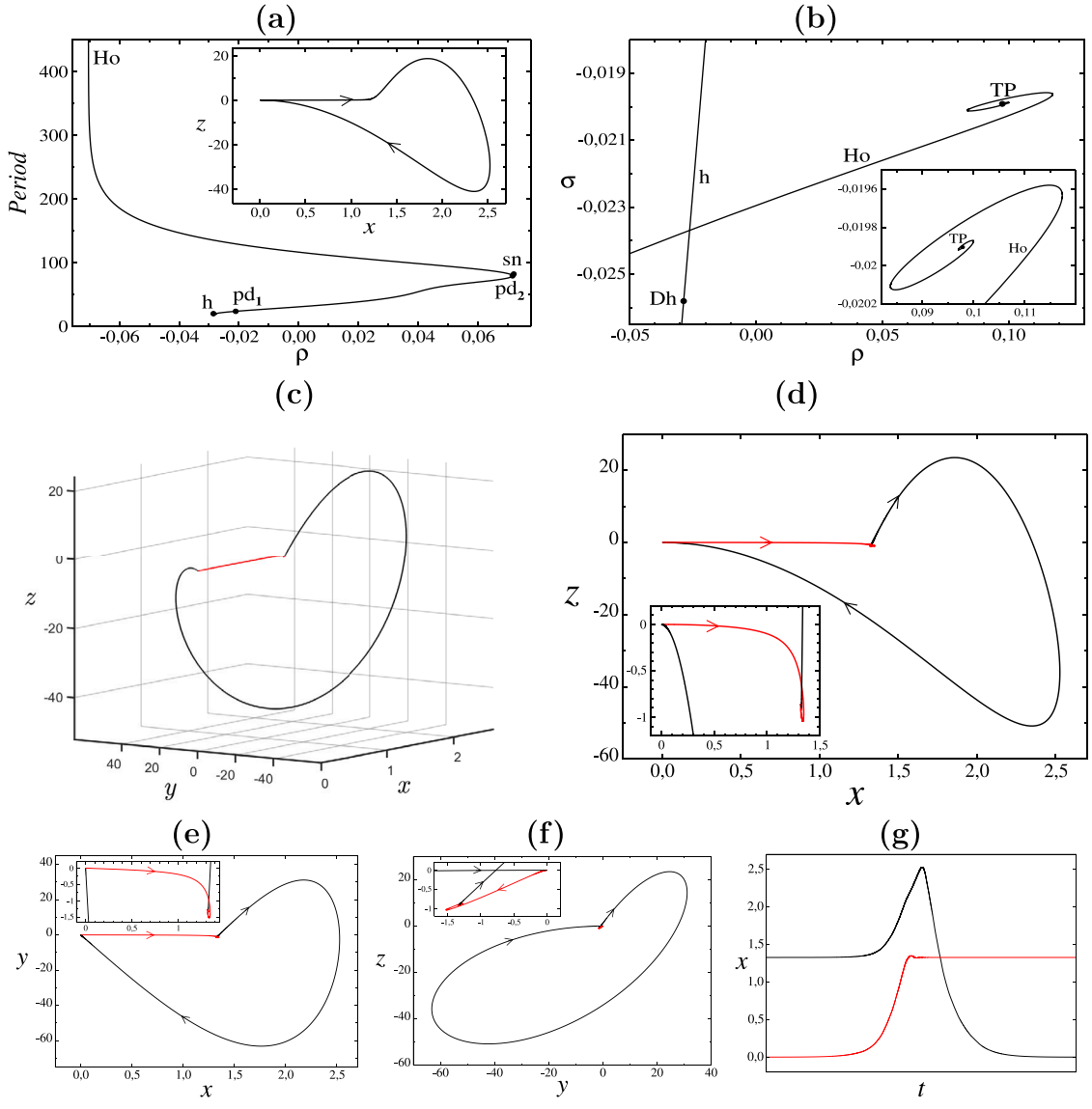

Fig. 2. For $b = -1.95$: (a) When $\sigma = -0.025$, bifurcation diagram of the asymmetric periodic orbit born in the Hopf bifurcation of the nontrivial equilibria **h**. It ends in a homoclinic connection to the origin **Ho**. The projection of this global connection in the x-z plane appears in the inset. (b) Partial bifurcation set with the curves **h** and **Ho**. The curve **Ho** emerges spiraling from a T-point **TP**, placed at $(\rho, \sigma) \approx (0.0977841, -0.0199045)$. (c) T-point heteroclinic cycle in the phase space. Projection of the T-point heteroclinic loop onto the: (d) x-z plane; (e) x-y plane; (f) y-z plane. (g) Temporal profile $x(t)$ of the T-point heteroclinic loop **TP**. The black (alt., red) orbit corresponds to the intersection between the one-dimensional (alt., two-dimensional) manifolds of the equilibria. Note that, because of the symmetry, all these orbits come in pairs.

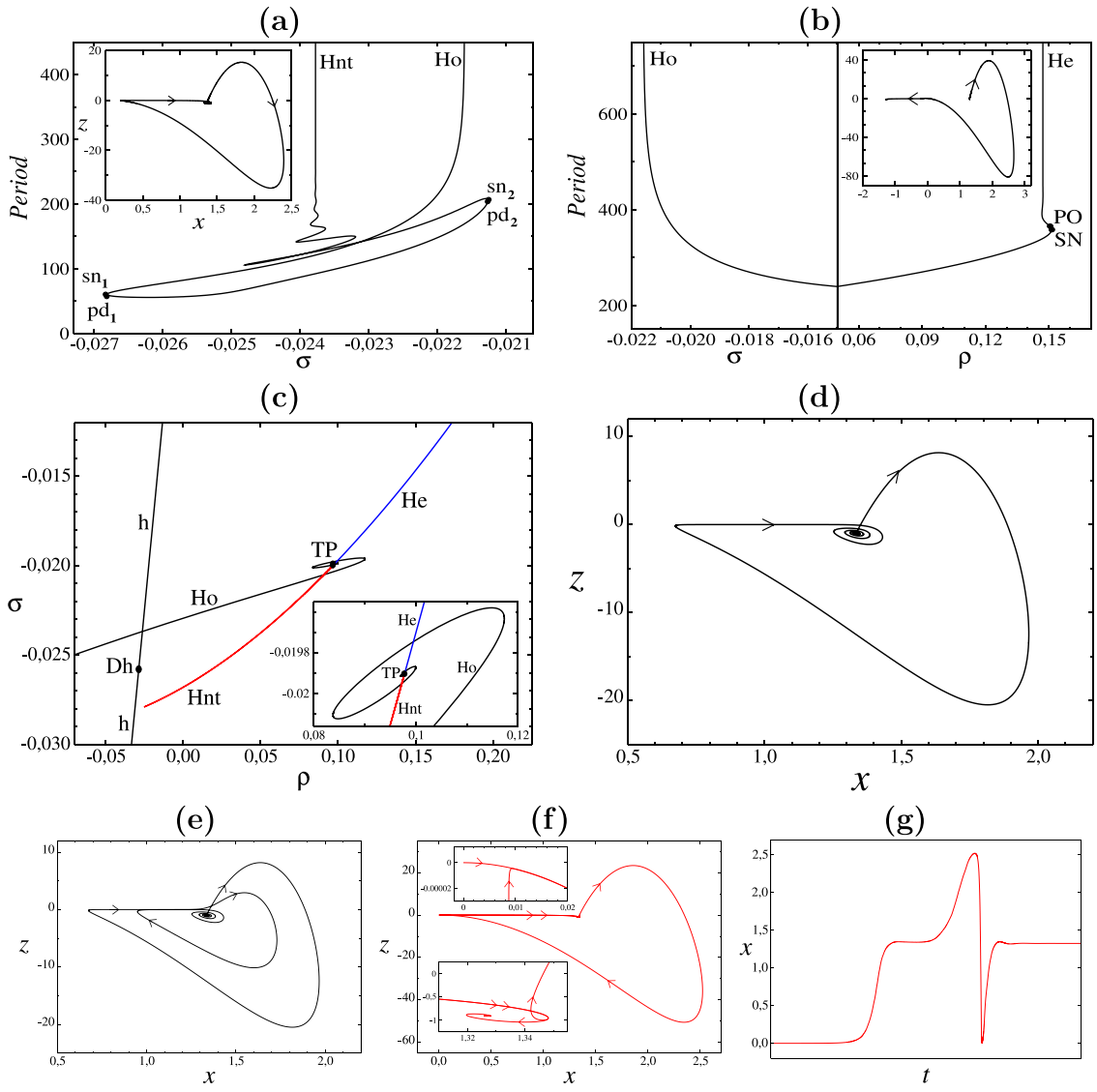

Fig. 3. For $b = -1.95$: (a) Bifurcation diagram for $\rho = 0.05$ of the asymmetric periodic orbit born in the homoclinic bifurcation of the origin **Ho**, which exists when $\sigma \approx -0.021601037$. It ends in a homoclinic connection to the nontrivial equilibria **Hnt**. The projection of this global connection in the x-z plane appears in the inset. (b) Bifurcation diagram of the symmetric periodic orbit emerged from **Ho** for $\rho = 0.05$ in $(\sigma, Period)$ and for $\sigma = -0.015$ in $(\rho, Period)$. The projection on the x-z plane of the heteroclinic connection **He** appears in the inset. (c) Partial bifurcation set in a neighborhood of the T-point **TP** with the curves **Ho**, **Hnt** and **He**. Projection onto the x-z plane of: (d) The homoclinic orbit to the nontrivial equilibria, for $(\rho, \sigma) \approx (0, -0.01966654)$; (e) The double-pulse homoclinic orbit to the nontrivial equilibria, for $(\rho, \sigma) \approx (0, -0.01966654)$; (f) The heteroclinic orbit which corresponds to the intersection of the 2D manifolds of the equilibria, at the endpoint **TP** of the double-pulse branch of the curve **Hnt**. (g) Temporal profile $x(t)$ of this heteroclinic orbit. (For interpretation of the references to color in this figure legend, the reader is referred to the web version of this article.)

after undergoing such bifurcations ends in a homoclinic connection to the origin **Ho**, when $\rho \approx -0.0703336$, whose projection onto the x-z plane appears in the inset.

Starting from these bifurcation points, we obtain the partial bifurcation set for $b = -1.95$ (see Fig. 2(b)), with the curves **h** (Hopf bifurcation of the nontrivial equilibria) and **Ho** (homoclinic connections to the origin). As in [11, Fig. 11], a first-order degeneracy **Dh** appears on the curve **h** (see [10]), when $(\rho, \sigma) \approx (-0.0286006, -0.0258081)$. The Hopf bifurcation is subcritical (a pair of repulsive asymmetric periodic orbits arises) above the point **Dh** and supercritical (a pair of saddle asymmetric periodic orbits emerges) at the remaining points of the curve shown in the figure. It is important to note that, since we are going to move in a region where $b < -1$ and $\sigma < 0$, the divergence of the Lorenz system, $div(x, y, z) = -(b + \sigma + 1)$, will always be positive, so that attractive periodic orbits cannot exist. In turn, we see that the curve **Ho** spirals to end at point **TP**, placed at $(\rho, \sigma) \approx (0.0977841, -0.0199045)$. This behavior of the homoclinic curve suggests that at the point **TP** there could exist a T-point heteroclinic cycle.

To corroborate this, at the endpoint of the curve **Ho**, we represent the homoclinic connection in the phase space and the corresponding temporal profiles of the three state variables. In this way we confirm that it is a T-point. Indeed (see Fig. 2(c)), a branch of the one-dimensional unstable manifold of the equilibrium E_+ coincides with a branch of the one-dimensional stable manifold of the origin (this codimension-two heteroclinic connection is drawn in black, as we will always do throughout this work). At the same time, the intersection between the two-dimensional unstable manifold of the origin and the two-dimensional stable manifold of E_+ (this codimension-zero heteroclinic connection is drawn in red, as we will always do throughout this paper) closes the heteroclinic cycle. To better visualize the geometric shape of this heteroclinic cycle, in Figs. 2(d), 2(e) and 2(f), we draw its projections on the coordinate planes. In addition, in Fig. 2(g), we represent the $x(t)$ profile of both heteroclinic connections.

We will now discuss some differences between the *classical* T-point (see Fig. 1(a)) and the new T-point (see Fig. 2(d)). First, we observe that the trajectory of the new T-point occurs in the opposite direction

of time (for example, in the new T-point, the one-dimensional manifold emerges from E_+ and reaches the origin). If we look at the projection of the T-points in the x-z plane, two aspects of its geometry are of interest. Focusing on the variable x, in the *classical* T-point, the one-dimensional manifold emerges from the origin towards the right ($x > 0$) but eventually enters the left equilibrium E_- (the one with $x < 0$). That is, the heteroclinic cycle does not connect the origin to the nontrivial equilibrium via the "shortest" path; it is not "direct". This is also the typical configuration in the T-point heteroclinic cycle of other systems, such as Shimizu-Morioka [3, Fig. 12], Chua [24], and modified van der Pol circuit [29] systems. In contrast, the new heteroclinic cycle is entirely contained in the region where $x > 0$, "directly" connecting both equilibria.

As we will theoretically demonstrate in the next section, the second geometric difference will have significant consequences for the bifurcation set. In the new T-point, the heteroclinic orbit corresponding to the intersection of the two-dimensional manifolds emerges from the origin tangential to the plane $z = 0$ (while, at the *classical* T-point, it enters the origin tangential to the z-axis). In this case, the eigenvalues of the Jacobian matrix at the origin are (see Eq. (2)): $\lambda_1 \approx -0.998$, $\lambda_2 \approx 0.018$, and $\lambda_3 \approx 1.95$. Therefore, since $\lambda_2 < \lambda_3$, the dominant direction near the origin in the unstable eigenspace is that of the eigenvector of λ_2, which lies in the x-y plane. This fact is very evident since $\lambda_2/\lambda_3 \approx 0.0092$ (see Fig. 2(d)).

To obtain the other two curves arising from the point **TP** (corresponding to homoclinic and heteroclinic connections to the nontrivial equilibria) we make two bifurcation diagrams. The first one, see Fig. 3(a), corresponds to the saddle asymmetric periodic orbit arising from **Ho**, which occurs at $(\rho, \sigma) \approx (0.05, -0.021601037)$. It exhibits a saddle–node bifurcation $\mathbf{sn_1}$ for $\sigma \approx -0.026810673922$. The repulsive periodic orbit arising from $\mathbf{sn_1}$ undergoes two period-doubling bifurcations $\mathbf{pd_1}$ when $\sigma \approx -0.026810673877$ (the second $\mathbf{pd_2}$ when $\sigma \approx -0.0212562847$) before collapsing at a new saddle–node bifurcation $\mathbf{sn_2}$ for $\sigma \approx -0.0212562846$. The saddle periodic orbit arising from $\mathbf{sn_2}$ undergoes further saddle–node and period-doubling bifurcations before disappearing at a homoclinic connection to the nontrivial equilibria **Hnt**, when $\sigma \approx -0.0237724$. The projection onto the x-z plane of this homoclinic connection appears in the inset.

The second bifurcation diagram, represented in Fig. 3(b), has been obtained by continuing in two steps the saddle symmetric periodic orbit which arises from the homoclinic connection **Ho**. In the first one (see the left part of the diagram), we fix $\rho = 0.05$ and represent Period versus σ, up to $\sigma = -0.015$ (this periodic orbit does not experience any bifurcation in the range of the figure). Now, in the second step (see the right part of the diagram), we fix $\sigma = -0.015$ and represent Period versus ρ, starting from $\rho = 0.05$. It exhibits various saddle–node (**SN**) and symmetry-breaking (**PPO**) bifurcations and ends in a heteroclinic connection **He** between the nontrivial equilibria, when $\rho \approx 0.147117$. We have marked the first **SN** and **PPO** bifurcations, which occurs for $\rho \approx 0.15118839496$ and $\rho \approx 0.15118839493$, respectively. The projection onto the x-z plane of this heteroclinic connection appears in the inset. We comment that, when ρ tends to $-\infty$, the period of these orbits tends to zero and its amplitude to ∞ (this behavior is similar to that reported in the Lorenz system for the so-called superluminal periodic orbits [42], when ρ tends to ∞).

Once the three global bifurcations arising from the point **TP** have been detected, we draw in Fig. 3(c) the partial bifurcation set around it, for $b = -1.95$. We can see how the curves **Ho** (homoclinic orbits to the origin), **Hnt** (homoclinic connections to the nontrivial equilibria; red color), and **He** (heteroclinic connections between the nontrivial equilibria; blue color) emerge from **TP**. The most outstanding fact is that the curves **Hnt** and **He** arise in opposite directions, a situation not previously found in the literature (compare with Fig. 1(b)). The next section will be devoted to theoretically justifying this new arrangement of the curves **Hnt** and **He**.

On the other hand, a noteworthy detail in Fig. 3(c) is that the curve **Hnt** starts and ends at the same point **TP** in the parameter plane. This is due to the existence of two different intersections of the two-dimensional manifolds of the equilibria (in [43,44], this situation is called bi-spiraling because there the homoclinic curve has a spiral shape). Indeed, the curve **Hnt** emerges from the point **TP** and has a turning point, when $(\rho, \sigma) \approx (-0.0251372, -0.0279116)$, such that the descending part (on which the homoclinic orbit of Fig. 3(d) occurs) and the ascending branch (on which the double-pulse homoclinic connection of Fig. 3(e) exists) are so close that they are indistinguishable (the descending branch is on the right side). Precisely the left branch of the curve **Hnt** (of double-pulse homoclinic connections) ends at the point **TP**. The new (and considerably more complex) intersection of the two-dimensional manifolds of the equilibria is shown in Fig. 3(f), with a portion of it lying very close to both the one-dimensional manifolds of the equilibria and the intersection of the two-dimensional manifolds depicted in Fig. 2(d). The two insets in Fig. 3(f), each located near an equilibrium, aim to clarify the nature of this trajectory. Additionally, its temporal profile $x(t)$, illustrated in Fig. 3(g), can be compared to the one presented in Fig. 2(g).

The following comments complete the information on the curves **Ho**, **Hnt** **He**. At all points on the curve **Hnt**, the nontrivial equilibria $E_\pm$ are saddle-focus. If we denote by $\delta_0 = \left|min(\lambda_2, \lambda_3)/\lambda_1\right|$, it holds that $\delta_0 < 1$ for all points on the curve **Ho** in the range of Fig. 3(c). The curve **He** exists between **TP** and the point $(\rho, \sigma) \approx (0.263157, 0)$. Finally, we mention that for $b = -1.95$ another curve of homoclinic connections to the origin arises from the point $(\rho, \sigma) = (1, -1)$, where the origin experiences a Takens–Bogdanov bifurcation. It exists in the $\sigma < -1$ zone and is similar to the **Ho** curve present in [11, Fig. 10].

3. A theoretical model

In this section, we aim to develop a theoretical model by constructing several Poincaré sections close to the main object of study, the T-point heteroclinic cycle. This model will provide, up to first order, the expression of the codimension-one global bifurcation curves emanating from the T-point, in a theoretical parameter plane with coordinates (d_1, d_2).

Specifically, we will explain that the curves of homoclinic and heteroclinic connections of the non-trivial equilibria emerge from the T-point in opposite directions. The Glendinning and Sparrow model [22] cannot account for this fact, so we propose to modify it appropriately to achieve our goal. The validity of the model is based on the C^1-linearity of the saddle-focus equilibrium (see [45]), on that of the real saddle equilibrium under generic conditions (see [37, Appendix A]), and on the first-order approximation of the global diffeomorphisms between the cross sections of the two equilibria. There are other alternative approaches to the study of real saddle equilibria that also include non-generic situations (see [46]).

A schematic representation of our theoretical model appears in Fig. 4. Initially, we consider only two equilibria, Q_1 and Q_2, which are connected by a heteroclinic cycle. This will allow us, by taking four cross-sections through the flow, to find the first-order expressions for the homoclinic curves of both equilibria. Next, we will use the system's invariance under the symmetry $(x, y, z) \to (-x, -y, z)$, which implies the existence of three equilibria: Q_1 (located at the origin) and the symmetric pair Q_2 and Q_2^{sim}. This symmetry also implies that there are two simultaneous T-point heteroclinic cycles (the one drawn and its symmetrical counterpart). From these cycles, two symmetric homoclinic connections to Q_1 and symmetric homoclinic orbits to Q_2 and Q_2^{sim} appear. In addition, a pair of symmetric heteroclinic connections exists between Q_2 and Q_2^{sim}.

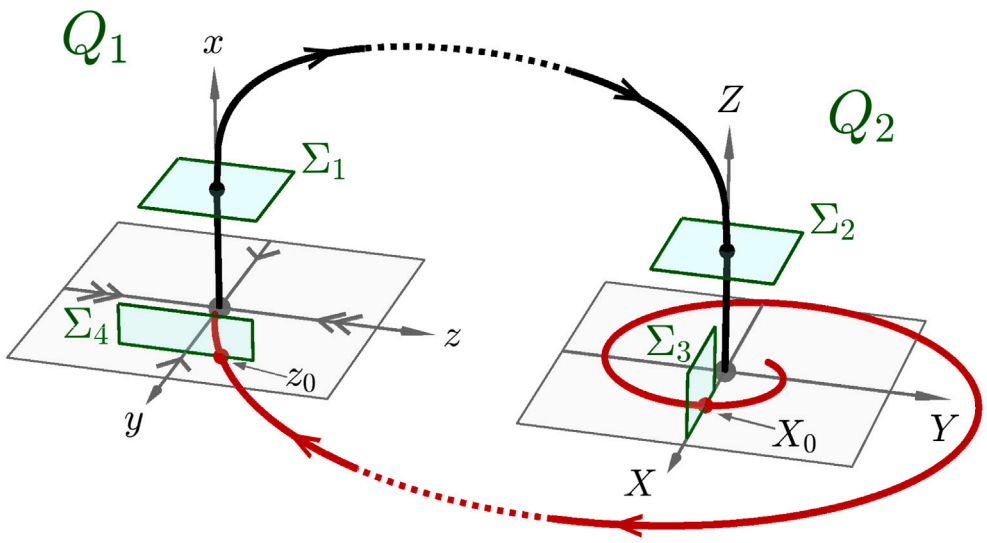

Fig. 4. Schematic heteroclinic loop between Q_1 and Q_2, showing the surfaces Σ_1, Σ_2, Σ_3, and Σ_4 used to construct the return map.

3.1. Maps

The main idea is to compute the linearized flow of the system in a tubular neighborhood of the heteroclinic cycle. In a vicinity of Q_1, which is a real saddle, we choose coordinates (x, y, z), such that the flow of the system is generated by the equations

$$\begin{cases} \dot{x} &= \lambda_1 x, \\ \dot{y} &= -\lambda_2 y, \\ \dot{z} &= -\lambda_3 z, \end{cases} \tag{3}$$

where $\lambda_1 > 0$ and $\lambda_3 > \lambda_2 > 0$.

Similarly, in a neighborhood of Q_2 (saddle-focus equilibrium) suitable coordinates (X, Y, Z) can be chosen in such a way that the flow is governed by the equations

$$\begin{cases} \dot{X} &= PX - \Omega Y, \\ \dot{Y} &= \Omega X + PY, \\ \dot{Z} &= -\Lambda Z, \end{cases} \tag{4}$$

where $P > 0$ (unstable focus), $\Lambda > 0$ (stable one-dimensional manifold). The sign of Ω is not fundamental in this study since it only indicates the direction of rotation.

In these coordinates, the local manifolds of the equilibria are rectified (coinciding with their linear manifolds). Thus, the stable two-dimensional manifold of Q_1 is locally contained in the $x = 0$ plane (the strong manifold is on the z axis and the weak manifold on the y axis), its unstable one-dimensional manifold in the x-axis, the unstable two-dimensional manifold of Q_2 in the $Z = 0$ plane, and its stable one-dimensional manifold in the Z-axis.

Now, using the local coordinates given above, the following four transversal sections to the flow in the neighborhoods of Q_1 and Q_2 can be defined (see Fig. 4 and also, for instance, [22,37,47]):

$$\begin{array}{rcl} \Sigma_1 &=& \left\{(x, y, z);\ x = h_x > 0\right\}, \\ \Sigma_2 &=& \{(X, Y, Z);\ Z = H > 0\}, \\ \Sigma_3 &=& \{(X, Y, Z);\ Y = 0\}, \\ \Sigma_4 &=& \left\{(x, y, z);\ y = h_y > 0\right\}, \end{array} \tag{5}$$

where h_x, h_y and H are small enough positive numbers.

Note that we focus in the flow near the intersection points of the T-point heteroclinic cycle with these four Poincaré sections. In the case of Σ_3, the neighborhood of the point $(X, Z) = (X_0, 0)$ must be small enough to avoid other intersections of the same orbit. The intersection point of the codimension-zero orbit of the T-point heteroclinic cycle with Σ_4 is $(x, z) = (0, z_0)$. Regarding the intersections of its codimension-two orbit with Σ_1 and Σ_2, they occur, respectively, at $(y, z) = (0, 0)$ and at $(X, Y) = (0, 0)$.

Now the flow applications between the different sections are obtained. First of all, we have $T_1 : \Sigma_4 \to \Sigma_1$, $T_1(x, h_y, z) = (h_x, y', z')$, $x > 0$, where

$$\begin{pmatrix} y' \\ z' \end{pmatrix} = \begin{pmatrix} qx^\gamma \\ pzx^\delta \end{pmatrix}, \tag{6}$$

being

$$\delta = \frac{\lambda_3}{\lambda_1}, \quad \gamma = \frac{\lambda_2}{\lambda_1}, \quad q = h_y h_x^{-\gamma}, \quad p = h_x^{-\delta},$$

with $\delta > \gamma > 0$, because $\lambda_3 > \lambda_2$ and $\lambda_1 > 0$. Note that to construct T_1 it is enough to integrate the system (3).

The transition $T_2 : \Sigma_1 \to \Sigma_2$ is given by $T_2(h_x, y', z') = (X', Y', H)$, where

$$\begin{pmatrix} X' \\ Y' \end{pmatrix} = \begin{pmatrix} d_1 \\ d_2 \end{pmatrix} + \begin{pmatrix} a & b \\ c & d \end{pmatrix} \begin{pmatrix} y' \\ z' \end{pmatrix}, \tag{7}$$

with $ad - bc \neq 0$ (linear diffeomorphism) and where d_1 and d_2 are the main parameters of the model.

The third map, $T_3 : \Sigma_3 \to \Sigma_2$, is given by $T_3(X, 0, Z) = (X', Y', H)$, where

$$\begin{pmatrix} X' \\ Y' \end{pmatrix} = XZ^\Delta H^{-\Delta} \begin{pmatrix} \cos(\Theta \log Z + \Phi) \\ \sin(\Theta \log Z + \Phi) \end{pmatrix}, \tag{8}$$

with

$$\Delta = \frac{P}{\Lambda}, \quad \Theta = \frac{\Omega}{\Lambda}, \quad \Phi = \frac{-\Omega}{\Lambda} \log H = -\Theta \log H.$$

Note that the direction of the flow is from Σ_2 to Σ_3. However, to simplify the computations, we calculate the inverse map.

Finally, we have $T_4 : \Sigma_3 \to \Sigma_4$, $T_4(X, 0, Z) = (x, h_y, z)$, being

$$\begin{pmatrix} x \\ z \end{pmatrix} = \begin{pmatrix} 0 \\ z_0 \end{pmatrix} + \begin{pmatrix} A & B \\ C & D \end{pmatrix} \begin{pmatrix} X - X_0 \\ Z \end{pmatrix}, \tag{9}$$

where $AD - BC > 0$ (orientation-preserving linear diffeomorphism), $X_0 > 0$, $A \neq 0$. If it were $A = 0$, then $Z = 0$ would be mapped into $x = 0$ for all X, resulting in the coincidence of the two-dimensional manifolds and the absence of a transversal intersection.

3.2. Global connections

Once the different transition maps have been defined, we then obtain the conditions for global connections to exist. First, the

codimension-two heteroclinic orbit of the T-point cycle is given by the trivial condition $T_2(h_x,0,0)=(0,0,H)$, which implies $(d_1,d_2)=(0,0)$.

Second, the condition for the existence of a homoclinic orbit to Q_1 is

$$T_4(T_3^{-1}(T_2(h_x,0,0)))=(0,h_y,z).$$

Since $T_2(h_x,0,0)=(d_1,d_2,H)$, the condition becomes $T_4(T_3^{-1}(d_1,d_2,H))=(0,h_y,z)$. Now, there exist a point $(X,0,Z)\in\Sigma_3$ such that $T_3^{-1}(d_1,d_2,H)=(X,0,Z)$, or equivalently,

$$\begin{pmatrix}d_1\\d_2\end{pmatrix}=XZ^{\Delta}H^{-\Delta}\begin{pmatrix}\cos(\Theta\log Z+\Phi)\\ \sin(\Theta\log Z+\Phi)\end{pmatrix}. \tag{10}$$

The condition $T_4(X,0,Z)=(0,h_y,z)$ implies, equating the first components, that $0=A(X-X_0)+BZ$, from which we obtain $X=X_0-\frac{B}{A}Z$ (recall that $A\neq 0$). Returning to the expression (10), we have

$$\begin{pmatrix}d_1\\d_2\end{pmatrix}=\left(X_0-\frac{B}{A}Z\right)Z^{\Delta}H^{-\Delta}\begin{pmatrix}\cos(\Theta\log Z+\Phi)\\ \sin(\Theta\log Z+\Phi)\end{pmatrix}. \tag{11}$$

Therefore, up to first order, the curve of homoclinic connections to Q_1, $\mathbf{HomQ_1}$, is a logarithmic spiral around $(d_1,d_2)=(0,0)$ (see Fig. 5).

Third, the condition for the existence of a homoclinic connection to Q_2 is

$$T_2(T_1(T_4(X,0,0)))=(0,0,H). \tag{12}$$

In order for this to occur there must exist a point $(x,h_y,z)\in\Sigma_4$, with $x>0$ such that $T_4(X,0,0)=(x,h_y,z)$. The inequality $x>0$ is a necessary condition for the flow to reach a neighborhood of Q_2 instead of the symmetric equilibrium Q_2^{sim}.

The expression for the map T_4, leads to

$$\begin{pmatrix}x\\z\end{pmatrix}=\begin{pmatrix}0\\z_0\end{pmatrix}+\begin{pmatrix}A&B\\C&D\end{pmatrix}\begin{pmatrix}X-X_0\\0\end{pmatrix}=\begin{pmatrix}A(X-X_0)\\z_0+C(X-X_0)\end{pmatrix}, \tag{13}$$

and, therefore, $z=z_0+\frac{C}{A}x$. By T_1, this point (x,h_y,z) is mapped into a $(h_x,y',z')\in\Sigma_1$ such that

$$\begin{pmatrix}y'\\z'\end{pmatrix}=\begin{pmatrix}qx^{\gamma}\\pzx^{\delta}\end{pmatrix}=\begin{pmatrix}qx^{\gamma}\\p\left(z_0+\frac{C}{A}x\right)x^{\delta}\end{pmatrix}. \tag{14}$$

Finally, this point has to be transformed into $(0,0,H)\in\Sigma_2$ (one-dimensional manifold) by T_2, that is,

$$\begin{pmatrix}0\\0\end{pmatrix}=\begin{pmatrix}d_1\\d_2\end{pmatrix}+\begin{pmatrix}a&b\\c&d\end{pmatrix}\begin{pmatrix}qx^{\gamma}\\p\left(z_0+\frac{C}{A}x\right)x^{\delta}\end{pmatrix}. \tag{15}$$

Solving for (d_1,d_2) we obtain

$$\begin{pmatrix}d_1\\d_2\end{pmatrix}=-x^{\gamma}\begin{pmatrix}aq+b\left(z_0+\frac{C}{A}x\right)x^{\delta-\gamma}\\cq+d\left(z_0+\frac{C}{A}x\right)x^{\delta-\gamma}\end{pmatrix}=-qx^{\gamma}\begin{pmatrix}a\\c\end{pmatrix}+o(x^{\gamma}), \tag{16}$$

where $x>0$ and $\delta>\gamma$. This is the expression of the curve of homoclinic connections of Q_2, $\mathbf{HomQ_2}$, in the (d_1,d_2)-parameter plane (see Fig. 5). When $x\to 0^+$, the curve tends to $(d_1,d_2)=(0,0)$, with the direction of the vector $\begin{pmatrix}a\\c\end{pmatrix}$ determined by $ad_1<0$, $cd_2<0$.

Fourth, since the Lorenz system has the symmetry $(x,y,z)\to(-x,-y,z)$, this fact must be incorporated into the model. Finally, we summarize the principal effects of this symmetry in the following lines:

- Equilibrium Q_1 is located at the origin, and equilibrium Q_2 has another symmetrical one, which we have called Q_2^{sim}.
- For $(d_1,d_2)=(0,0)$, there are two simultaneous T-point heteroclinic cycles, which are symmetrical to each other.
- The homoclinic orbit of the origin is associated with another symmetrical one. Therefore, on the curve $\mathbf{HomQ_1}$ given to first order in (11), there is a double homoclinic connection of Q_1.
- The homoclinic orbit of the non-trivial equilibrium Q_2 is associated with another symmetrical one, that corresponds to Q_2^{sim}. This occurs on the same curve given up to first order in (16), $\mathbf{HomQ_2}$.

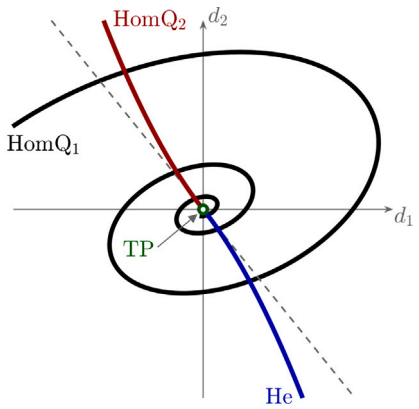

Fig. 5. Partial bifurcation set in the (d_1,d_2)-plane, in a neighborhood of the T-point, **TP**. Curve $\mathbf{HomQ_1}$ (black) has a spiral shape. The curves $\mathbf{HomQ_2}$ (red) and **He** (blue) emerge in opposite directions. (For interpretation of the references to color in this figure legend, the reader is referred to the web version of this article.)

- The existence of heteroclinic connections of codimension one between the equilibria Q_2 and Q_2^{sim} is possible.
  In fact, for such a heteroclinic connection to occur, the following conditions must hold. First, a curve of the two-dimensional manifold of Q_2 that corresponds to a point $(X,0,0)\in\Sigma_3$ must reach a neighborhood of Q_1, but entering through a point $(x,h_y,z)\in\Sigma_4$ where, in this case, $x<0$. By following the same reasoning used for the homoclinic connections to Q_2, from the expression of T_4 one can obtain the equality $z=z_0+\frac{C}{A}x$.
  Now, by the symmetry, the orbit corresponding to this point $(x,h_y,z)\in\Sigma_4$ with $x<0$ reaches the point Q_2^{sim} by its one-dimensional stable manifold if, and only if, the orbit corresponding to the symmetric point $(-x,-h_y,z)\in\Sigma_4^{sim}:=\{(-x,y,z);\ y=-h_y<0, x<0\}$ reaches the point Q_2 by its one-dimensional stable manifold. This can be written as

$$T_2(T_1^{sim}(-x,-h_y,z))=(0,0,H)\in\Sigma_2, \tag{17}$$

  where $T_1^{sim}:\Sigma_4^{sim}\to\Sigma_1$ is given by $T_1^{sim}(-x,-h_y,z)=(h_x,-q(-x)^{\gamma},pz(-x)^{\delta})$. This expression for the map T_1^{sim} is obtained by integrating (3), analogously to T_1.
  Analogous to the homoclinic connections of Q_2, from Eq. (17) and given that $z=z_0+\frac{C}{A}x$, it follows that

$$\begin{pmatrix}d_1\\d_2\end{pmatrix}=-(-x)^{\gamma}\begin{pmatrix}-aq+bp\left(z_0+\frac{C}{A}x\right)(-x)^{\delta-\gamma}\\-cq+dp\left(z_0+\frac{C}{A}x\right)(-x)^{\delta-\gamma}\end{pmatrix}\approx q(-x)^{\gamma}\begin{pmatrix}a\\c\end{pmatrix}. \tag{18}$$

  When $x\to 0^-$, this curve **He** tends to the T-point $(d_1,d_2)=(0,0)$, with the direction of the vector $\begin{pmatrix}a\\c\end{pmatrix}$ determined by $ad_1>0$, $cd_2>0$, that is, in the opposite direction to the Q_2 homoclinic curve. Up to first order, the homoclinic and heteroclinic curves of Q_2 and Q_2^{sim}, $\mathbf{HomQ_2}$ and **He**, are symmetric in the (d_1,d_2)-plane, with the symmetry $(d_1,d_2)\to(-d_1,-d_2)$.

Fig. 5 shows the partial bifurcation set in the (d_1,d_2)-plane in a neighborhood of the T-point, obtained using the model.

4. T-points in a Lorenz-like system

The aim of this section is to determine whether the *classical* T-point appearing in the Lorenz system (see Fig. 1) can experience a degeneration (because the origin has a double eigenvalue), such that the intersection of the two-dimensional manifolds enters the origin tangent to the plane $z=0$ and that, consequently, the curves **Hnt** and

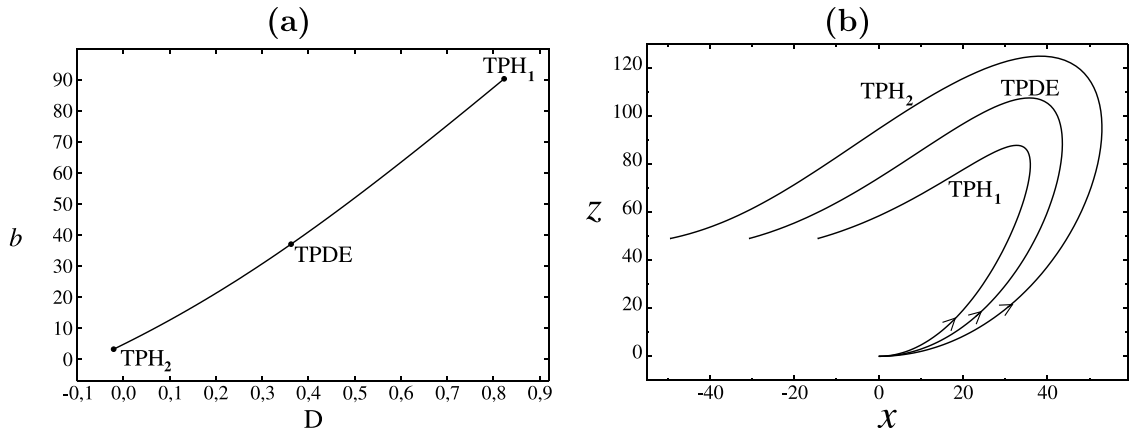

Fig. 6. For $\rho = 50$: (a) Projection onto the (D, b)-plane of the curve of principal T-points. It is bounded by two T-point-Hopf bifurcations, **TPH$_1$** and **TPH$_2$** and a degeneracy occurs at **TPDE** (because the origin has a double eigenvalue). (b) Projection onto the x-z plane of three heteroclinic orbits formed by the one-dimensional manifolds of the equilibria, which exist at the points **TPH$_1$**, **TPDE** and **TPH$_2$**.

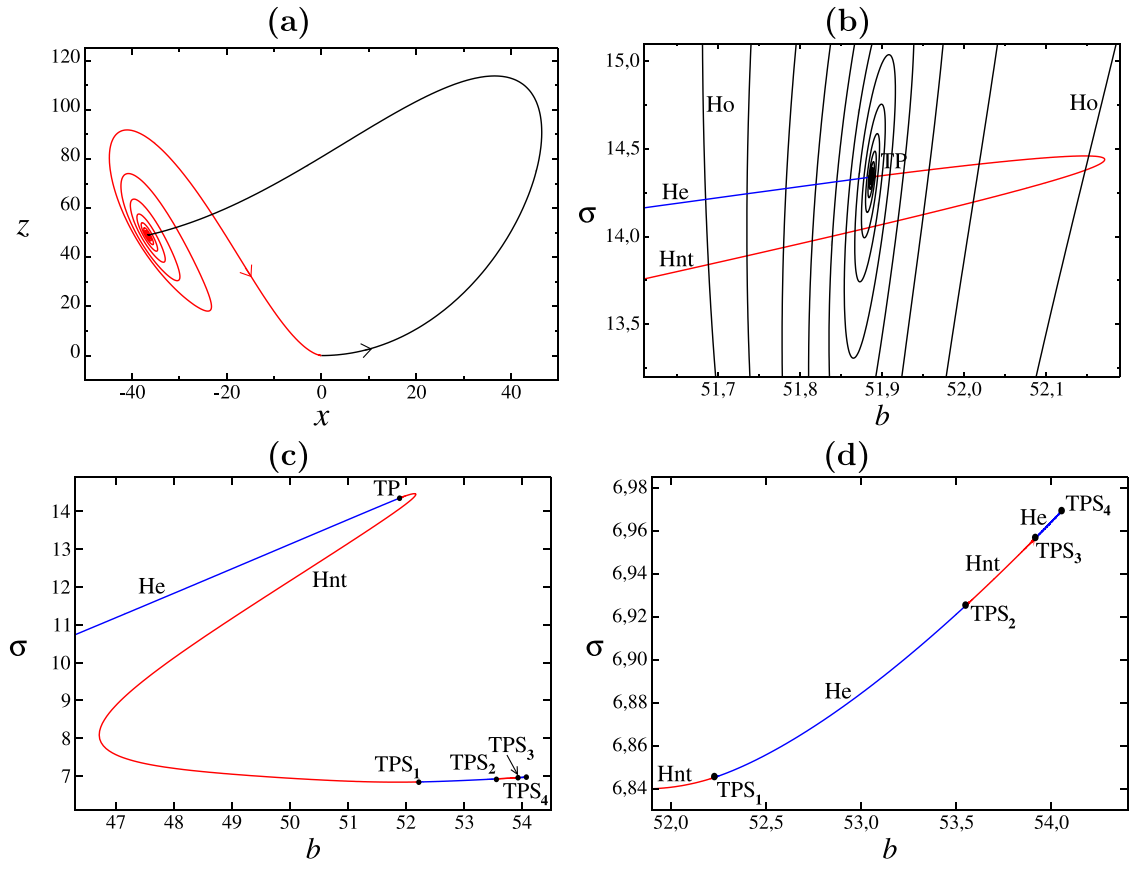

Fig. 7. For $\rho = 50$ and $D = 0.5$: (a) Projection onto the x-z plane of the principal T-point heteroclinic cycle, which exists when $(b, \sigma) \approx (51.887349, 14.339606)$. (b) Partial bifurcation set in the (b, σ)-plane, in a neighborhood of the T-point. Three curves of global connections emerge, namely, **Ho**, **Hnt** and **He**. Note that the curves **Hnt** and **He** arise in opposite directions. (c) Partial bifurcation set of curves **Hnt** and **He** joining the points **TP**, **TPS$_1$**, **TPS$_2$**, **TPS$_3$**, and **TPS$_4$**. (d) Zoom of panel (c) with the sequence of secondary T-points.

He arise from the point **TP** in opposite directions. First of all, we have verified on the curve of *classical* T-points in the (ρ, b, σ) parameter space of the Lorenz system that, for values $\rho \leq 1000$, it is always satisfied $\lambda_1 < \lambda_3 < 0 < \lambda_2$ (see Eq. (2)). Therefore, the degeneration $\lambda_1 = \lambda_3$ does not appear in that interval.

Based on this numerical evidence, we are going to search for that degeneracy in the Lorenz-like system [48]

$$\begin{aligned} \dot{x} &= \sigma(y - x), \\ \dot{y} &= \rho x - y - xz, \\ \dot{z} &= -bz + xy + Dz^2, \end{aligned} \tag{19}$$

where $D \in \mathbb{R}$, so that the Lorenz system is embedded in this one when $D = 0$. This system exhibits the same symmetry as the Lorenz system and can have up to four equilibria (a new one, E_1, appears on the z-axis when $D \neq 0$):

$$E_0 = (0, 0, 0), \quad E_1 = (0, 0, b/D), \quad E_\pm = \left(\pm\sqrt{K}, \pm\sqrt{K}, \rho - 1\right),$$

where $K = b(\rho - 1) - D(\rho - 1)^2 > 0$.

In this case, the T-point heteroclinic cycle connects the origin E_0 with the equilibria $E_\pm$. Note that the Jacobian matrix of E_0 is the same as in the Lorenz system, i.e. its eigenvalues are those given in Eq. (2).

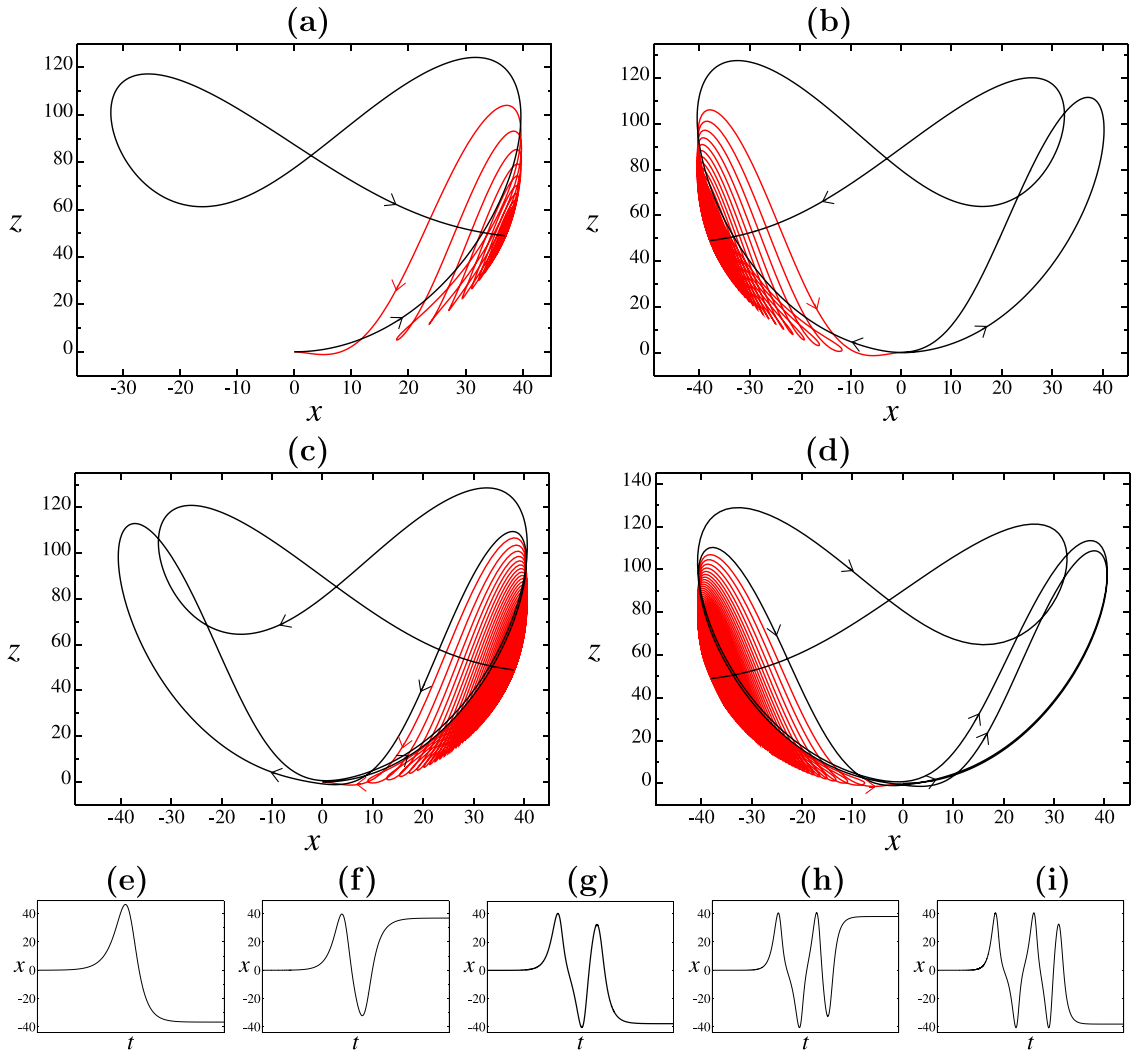

Fig. 8. For $\rho = 50$, projection onto the x-z plane of the T-point heteroclinic cycle: (a) $\mathbf{TPS_1}$, which exists when $(b,\sigma) \approx (52.230551, 6.845219)$. (b) $\mathbf{TPS_2}$, located at $(b,\sigma) \approx (53.557422, 6.925753)$. (c) $\mathbf{TPS_3}$, which exists when $(b,\sigma) \approx (53.910252, 6.956013)$. (d) $\mathbf{TPS_4}$, placed at $(b,\sigma) \approx (54.049281, 6.968655)$. Temporal profile $x(t)$ of the heteroclinic connection formed by the one-dimensional manifolds of the equilibria of the T-point: (e) **TP**. (f) $\mathbf{TPS_1}$. (g) $\mathbf{TPS_2}$. (h) $\mathbf{TPS_3}$. (i) $\mathbf{TPS_4}$.

Setting $\rho = 50$, and starting from the T-point for $D = 0$, we obtain the curve of principal T-points in the (b,σ,D)-parameter space (a projection is drawn in Fig. 6(a)). It presents the degeneracy $\lambda_1 = \lambda_3 \approx -37.03$ when $(b,\sigma,D) \approx (37.0349, 15.5117, D_c)$, where $D_c \approx 0.362690$, point labeled **TPDE**. Therefore, for $D > D_c$, according to the analysis in Section 3, the curves **Hnt** and **He** must emerge from **TP** in opposite directions. We see that this curve of T-points is bounded by the points $\mathbf{TPH_1}$, placed at $(b,\sigma,D) \approx (3.23475, 18.3889, -0.0208826)$, and $\mathbf{TPH_2}$, situated at $(b,\sigma,D) \approx (90.2287, 11.6479, 0.823242)$, at which T-point-Hopf bifurcations appear (because non-trivial equilibria $E_\pm$ undergo a Hopf bifurcation) [10]. In Fig. 6(b), we show the projection of the heteroclinic connections formed by the one-dimensional manifolds of the equilibria, which exist at the points $\mathbf{TPH_1}$, **TPDE** and $\mathbf{TPH_2}$.

Given the above, let us begin our numerical study by setting $\rho = 50$ and $D = 0.5 > D_c$. Thus, in Fig. 7(a) we show the projection on the x-z plane of the principal T-point, which exists when $(b,\sigma) \approx (51.887349, 14.339606)$. In the partial bifurcation set in the vicinity of the principal T-point **TP** (see Fig. 7(b)) we see the curves **Ho** (which has a spiral shape), **Hnt**, and **He**. These last two arise in opposite directions, as was shown in Section 3. As a curiosity, at the T-points of this system (always considering the orbit of the one-dimensional manifold of the origin that goes out towards the zone $x > 0$), it is verified that if the intersection between the two-dimensional manifolds reaches the origin with $x < 0$ and $y > 0$, then the curve **Hnt** arises to the right of **TP** while the curve **He** does so to the left (see Figs. 7(a) and 7(b)).

We will now focus (see Fig. 7(c)) on the curve **Hnt** since it will allow us to find a sequence of secondary T-points (T-points where one-dimensional manifolds are more "complicated" than those of principal T-point). Indeed, the curve **Hnt** arrives from the left at the secondary T-point $\mathbf{TPS_1}$, which exists when $(b,\sigma) \approx (52.230551, 6.845219)$, whose heteroclinic cycle is drawn in Fig. 8(a) (we observe that the intersection between the two-dimensional manifolds reaches the origin with $x > 0$ and $y < 0$). From $\mathbf{TPS_1}$ a heteroclinic curve **He** emerges on the right, which in turn reaches from the left side to the secondary T-point $\mathbf{TPS_2}$, located at $(b,\sigma) \approx (53.557422, 6.925753)$ (the corresponding heteroclinic cycle is drawn in Fig. 8(b); in this case, the intersection between the two-dimensional manifolds reaches the origin with $x < 0$ and $y > 0$). In turn, a homoclinic curve **Hnt** arises from the right of $\mathbf{TPS_2}$ and arrives from the left at the next secondary T-point $\mathbf{TPS_3}$, which exists when $(b,\sigma) \approx (53.910252, 6.956013)$ (its heteroclinic cycle appears in Fig. 8(c), where we see that the intersection between the two-dimensional manifolds reaches the origin with $x > 0$ and $y < 0$). From $\mathbf{TPS_3}$, to the right, a new heteroclinic curve **He** emerges which ends when it reaches the next secondary T point $\mathbf{TPS_4}$ on the left, located at $(b,\sigma) \approx (54.049281, 6.968655)$ (its heteroclinic cycle appears in Fig. 8(d); in this case, the intersection between the two-dimensional manifolds reaches the origin with $x < 0$ and $y > 0$). Although we have had

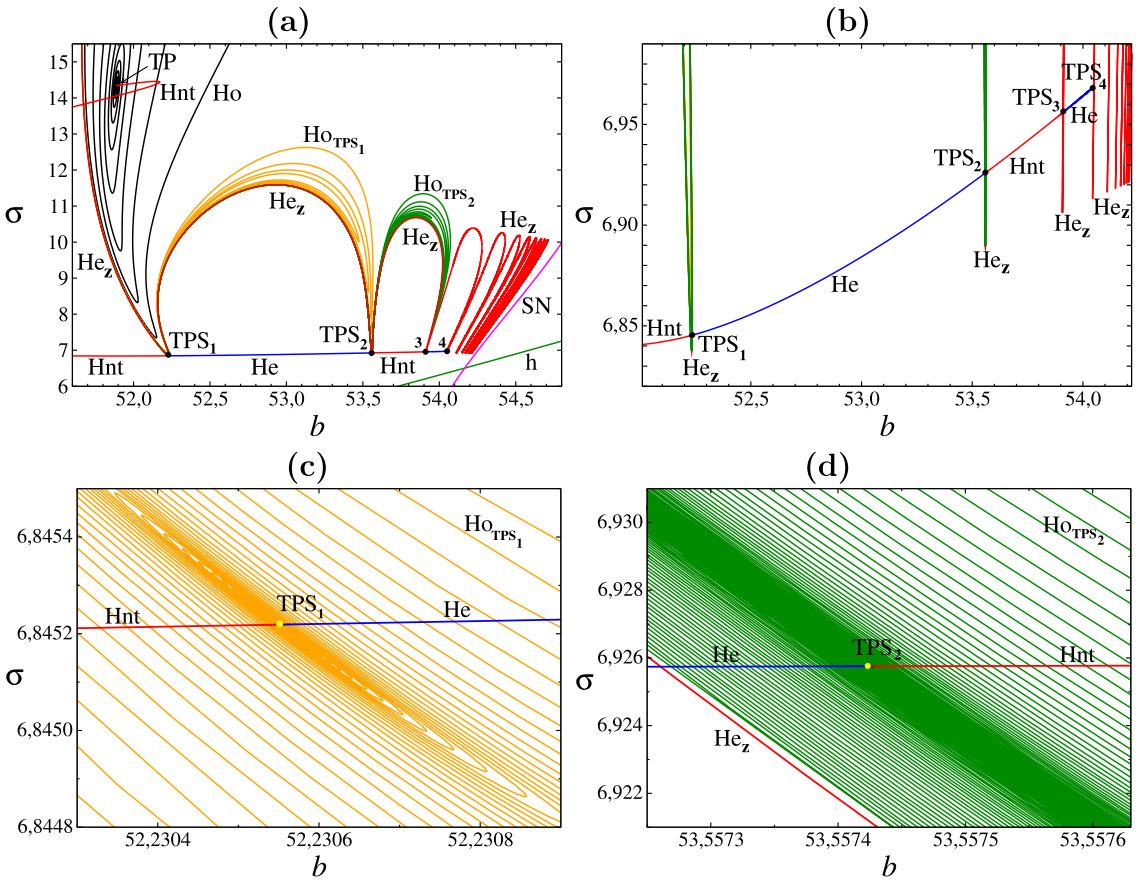

Fig. 9. For $\rho = 50$, $D = 0.5$: (a) Partial bifurcation set with the curves **h** (Hopf bifurcation of the nontrivial equilibria $E_{\pm}$), **SN** (saddle–node bifurcations of symmetric periodic orbits), **Ho**, $\mathbf{Ho_{TPS_1}}$, $\mathbf{Ho_{TPS_2}}$ (curves of homoclinic orbits to the origin, drawn in black, orange, and green, respectively), $\mathbf{He_z}$ (heteroclinic connections between E_0 and E_1), **He** (heteroclinic connections between $E_{\pm}$) and **Hnt** (homoclinic connections to the nontrivial equilibria $E_{\pm}$). (b) Zoom of panel (a). Zoom of panel (b) in a neighborhood of the secondary T-point: (c) $\mathbf{TPS_1}$. (d) $\mathbf{TPS_2}$. (For interpretation of the references to color in this figure legend, the reader is referred to the web version of this article.)

numerical problems to continue it, the results of Section 3 guarantee that a new curve **Hnt** will emerge to the right of $\mathbf{TPS_4}$.

In Fig. 7(d) we enlarge the area in which the secondary T-points appear. In view of these results, we conjecture the existence of an infinite succession of secondary T-points joined by curves **Hnt** and **He**, where each of them emerges to the left or to the right of each T point, according to the analysis in Section 3. The profiles $x(t)$ of the one-dimensional manifolds of T-points **TP**, $\mathbf{TPS_1}$, $\mathbf{TPS_2}$, $\mathbf{TPS_3}$, and $\mathbf{TPS_4}$ appear in Figs. 8(e), 8(f), 8(g), 8(h), and 8(i), respectively. This helps to understand how the geometric structure of these heteroclinic orbits becomes increasingly complicated.

In [48] a double-zero bifurcation (a double-zero eigenvalue with geometric multiplicity two) in the system (19) was studied. There it was shown that a curve $\mathbf{He_z}$ of heteroclinic connections (between the two equilibria located on the z axis, E_0 and E_1) arises from this double-zero bifurcation. For $\rho = 50$, $D = 0.5$, the curve $\mathbf{He_z}$ accumulates on a line segment of a curve of saddle–node bifurcations of periodic orbits (see [48, Fig. 9]). We will see that the sequence of secondary T-points ($\mathbf{TPS_1}$, $\mathbf{TPS_2}$, $\mathbf{TPS_3}$ and $\mathbf{TPS_4}$) is inserted in an orderly manner in that partial bifurcation set in the (b, σ)-parameter plane.

To do this, we draw in Fig. 9(a) the curves **h** (Hopf bifurcation of the equilibria $E_{\pm}$; green), **SN** (saddle–node bifurcation of symmetric periodic orbits; magenta), **Ho** (homoclinic connections to the origin; black; emerged from the principal T-point **TP**), $\mathbf{Ho_{TPS_1}}$ (homoclinic connections to the origin; orange; emerged from $\mathbf{TPS_1}$), $\mathbf{Ho_{TPS_2}}$ (homoclinic connections to the origin; green; emerged from $\mathbf{TPS_2}$), $\mathbf{He_z}$ (heteroclinic connections between E_0 and E_1; red), **He** (heteroclinic connections between the equilibria $E_{\pm}$; blue), and **Hnt** (homoclinic connection to $E_{\pm}$; red) [48]. Note that, according to what was demonstrated in [47], the curves of homoclinic connections to the origin **Ho**, $\mathbf{Ho_{TPS_1}}$, $\mathbf{Ho_{TPS_2}}$,...,end in a degeneration that exists on the curve $\mathbf{He_z}$, located at $(b, \sigma) \approx (50.349119, 204.788065)$. As can be seen in Fig. 9(b), each of the points of the sequence $\mathbf{TPS_1}$, $\mathbf{TPS_2}$, $\mathbf{TPS_3}$ and $\mathbf{TPS_4}$ are located very close to each of the first four local minima that the curve $\mathbf{He_z}$ has when it approaches the curve **SN**. A new zoom in the vicinity of $\mathbf{TPS_1}$ and $\mathbf{TPS_2}$ appears in the figures Fig. 9(c) and Fig. 9(d), respectively. In them we can see how the curves **Hnt** and **He** arise, in opposite directions, from the points $\mathbf{TPS_1}$ and $\mathbf{TPS_2}$. It is important to note that the curve $\mathbf{He_z}$ acts as a barrier for the curves of homoclinic connections to the origin (**Ho**, $\mathbf{Ho_{TPS_1}}$, $\mathbf{Ho_{TPS_2}}$, ..., which emerge from the corresponding T-points, which in turn are very close to $\mathbf{He_z}$), since the heteroclinic orbit $\mathbf{He_z}$ also involves the origin. This causes the elongated and deformed shape that these spiral curves present.

Next, to conclude this section, we will study the bifurcation set in the (b, σ, D)-parameter space, for $\rho = 50$, which appears in the vicinity of the degenerate T-point. To do this, we intend to illustrate how the transition of the arrangement of the curves **Hnt** and **He** occurs when the degeneracy of the T-point appears for $D = D_c \approx 0.362690$. Specifically, we will look at six values of D (0, 0.3, D_c, 0.4, 0.5, 0.7) and we will compare, in the vicinity of the origin, how the arrangement of the heteroclinic connections is when they reach this equilibrium. We know that this is determined by the relationship between the eigenvalues λ_1 and $\lambda_3 = -b$ of the Jacobian matrix at the origin (see Eq. (2)). Then we consider, for example, its quotient $q_e = |\lambda_1|/|\lambda_3|$. Thus, if $q_e > 1$, the dominant direction is that of the eigenvector associated with λ_3, $v_3 = (0, 0, 1)^T$, so the entry to the origin occurs tangent to the z-axis. This means that the curves **Hnt** and **He** emerge from **TP** in the same

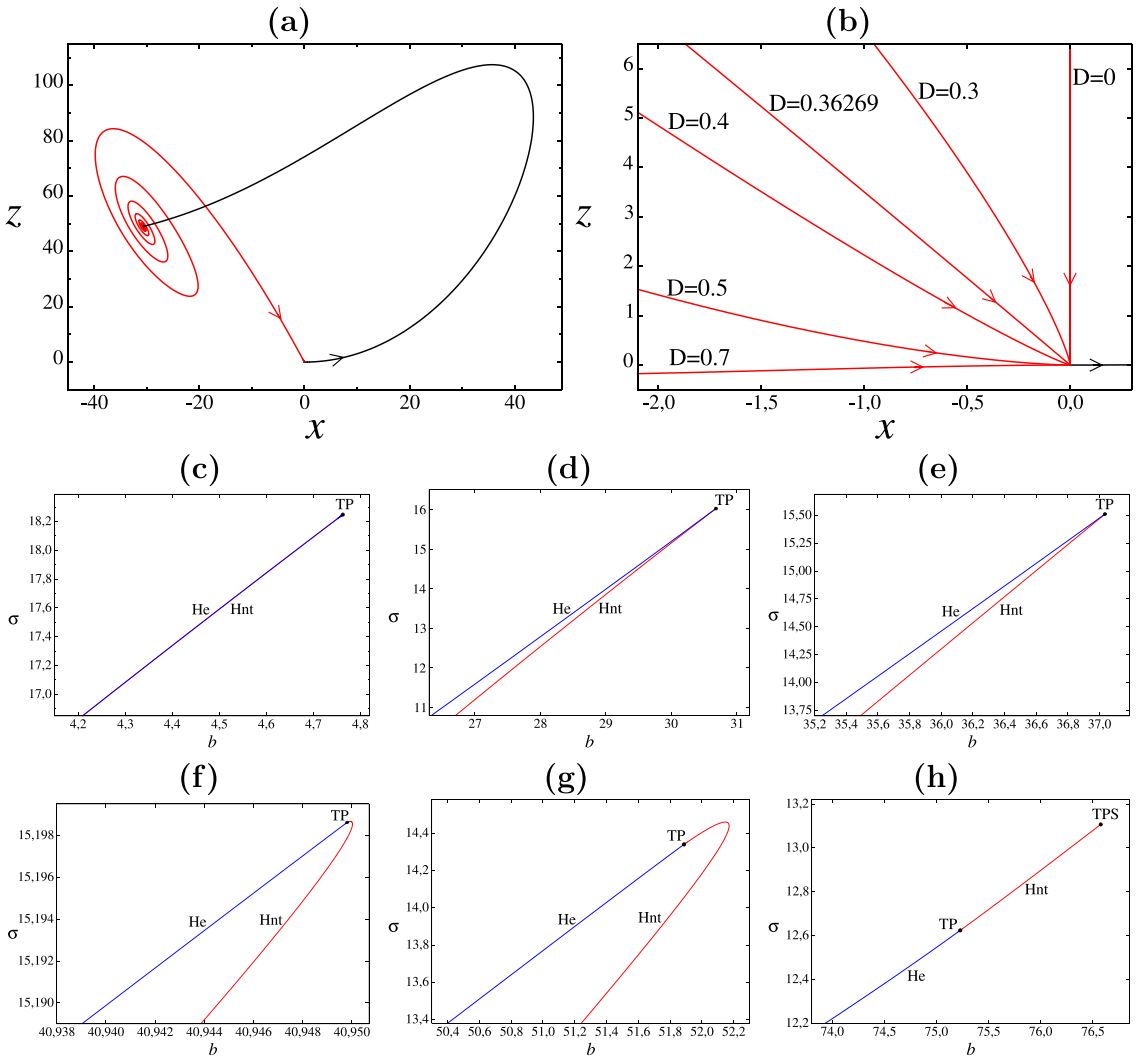

Fig. 10. For $\rho = 50$, projection onto the x-z plane of: (a) the principal T-point heteroclinic cycle which exists when $D = 0.362690$. The black (alt., red) orbit corresponds to the intersection between the one-dimensional (alt., two-dimensional) manifolds of the equilibria. (b) six principal T-points heteroclinic cycles (we only represent a zoom in a neighborhood of the origin) corresponding to $D = 0$, $D = 0.3$, $D = 0.362690$, $D = 0.4$, $D = 0.5$, and $D = 0.7$, respectively. Curves **Hnt** (in red) and **He** (in blue) in the (b, σ)-plane emerging from the corresponding T-point **TP** when: (c) $D = 0$. (d) $D = 0.3$. (e) $D = 0.362690$. (f) $D = 0.4$. (g) $D = 0.5$. (h) $D = 0.7$. (For interpretation of the references to color in this figure legend, the reader is referred to the web version of this article.)

Table 1
For $\rho = 50$, quotient $q_e = |\lambda_1|/|\lambda_3|$ for six values of the parameter D.

D	0	0.3	0.362690	0.4	0.5	0.7
q_e	8.62	1.23	1	0.893	0.680	0.433

direction (a well-known case of the Lorenz system, analyzed in [22]). However, if $q_e < 1$, the dominant direction is that of the eigenvector associated with λ_1, $v_1 = (v_{1x}, v_{1y}, 0)^T$ (where $v_{1x}v_{1y} < 0$) so the entry occurs tangent to the plane $z = 0$ (in the direction of v_1). This implies that the curves **Hnt** and **He** emerge from **TP** in opposite directions (situation studied in Section 3). In our specific case, the value of the quotient q_e for these six values of the parameter D appears in Table 1.

In Fig. 10(a), we represent the heteroclinic cycle of the principal T-point when the degeneration occurs, that is, when $D = D_c$. In this projection on the x-z plane we see that the direction of entry to the origin is not tangent to either the z-axis or the plane $z = 0$. In Fig. 10(b) we look at how the six heteroclinic orbits enter the origin (using the corresponding zoom). We see how, gradually, it goes from entering tangent to the z axis, when $D < D_c$, to doing so tangent to the vector v_1 (located in the plane $z = 0$), when $D > D_c$. Finally, in Figs. 10(c)-10(h), we see how the gradual change of the curve **Hnt** occurs: for values $D < D_c$ it emerges to the left of **TP** while when $D > D_c$ it emerges to the right. Just as we already saw in Fig. 7 that, for $D = 0.5$, the **Hnt** curve presents a turning point (to end up reaching the secondary T-point $\mathbf{TPS_1}$), this same thing happens for $D = 0.4$. However, when $D = 0.7$, the sequence of secondary T-points no longer exists (because they have disappeared in T-point-Hopf bifurcations). This causes the curve **Hnt** to no longer have a turning point and, specifically, to end at another secondary T-point **TPS**, which exists when $(b, \sigma) \approx (76.578311, 13.106772)$.

5. Conclusions

The three most important contributions of this work are the following. First of all (see Section 2), we have found a new kind of T-point heteroclinic cycle in the Lorenz system. We have seen that it not only has a different geometric structure in phase space from the *classical* T-point of that system, but also presents around it (in a parameter plane) a different bifurcation set. In this case, the curves of homoclinic and heteroclinic connections involving the non-trivial equilibria, **Hnt** and **He**, emerge from the T-point in opposite directions (in the only case known so far, those two global bifurcation curves emerge in the same

direction, as justified in [22]). Regardless of the above, the curve **Hnt** starts and ends at the same T-point in the parameter plane. This is due to the existence of two different intersections of the two-dimensional manifolds of the equilibria.

Secondly, analyzing the reason for one of those geometric differences, we have realized that it has to do with the eigenvalues of the Jacobian matrix at the origin, which is a real saddle. Indeed, while at the *classical* T-point, the heteroclinic orbit corresponding to the intersection of the two-dimensional manifolds arrives at the origin tangent to the z-axis (direction of the eigenvector corresponding to the eigenvalue λ_3, given in (2)), at the new T-point, this orbit leaves the origin tangent to the $z = 0$ plane (in the direction of the eigenvector corresponding to the eigenvalue λ_1). This situation is not contemplated in the Glendinning and Sparrow model [22]. To explain it, we modify this model appropriately (see Section 3), and we manage to demonstrate that the curves **Hnt** and **He** must emerge from the T-point in opposite directions.

Third, we have found a degenerate T-point (a global bifurcation of codimension 3), due to the appearance of a double eigenvalue in the Jacobian matrix of the equilibrium at the origin. To illustrate the changes in the bifurcation set in the vicinity of the degenerate T-point, we search for an appropriate system (see Section 4), which we obtain by introducing the term Dz^2 into the third equation of the Lorenz system (see Eq. (19)). In addition, we have found a sequence (which we conjecture to be infinite) of secondary T-points, connected by curves **Hnt** and **He**, which are very close to each of the local minima of the curve $\mathbf{He_z}$ (of heteroclinic connections between the two equilibria located on the z axis).

This work leaves several tasks open for the near future. As regards the new T-point found in the Lorenz system, it will be interesting to see the bifurcation set that it organizes around it (both global bifurcations and bifurcations of periodic orbits) as well as the possible degeneracies that it may present (for example, T-point-Hopf). Since the Chen and Lü systems are particular cases of the Lorenz system [49,50], it will not be difficult to determine whether the new T-point also exists in them.

It will also be stimulating to continue analyzing system (19), to find other organizing centers of the rich dynamics that it presents and relate them to other already known ones [47,48]. Likewise, considering the new T-point in system (19) can allow us to find new degenerations by also varying the parameter D.

CRediT authorship contribution statement

A. Algaba: Writing – review & editing, Writing – original draft, Methodology, Investigation, Formal analysis, Conceptualization. **F. Fernández-Sánchez:** Writing – review & editing, Writing – original draft, Methodology, Investigation, Formal analysis, Conceptualization. **M. Merino:** Writing – review & editing, Writing – original draft, Methodology, Investigation, Formal analysis, Conceptualization. **A.J. Rodríguez-Luis:** Writing – review & editing, Writing – original draft, Methodology, Investigation, Formal analysis, Conceptualization.

Funding sources

This work has been partially supported by the Ministerio de Ciencia, Innovación y Universidades, Spain (PID2021-123200NB-I00) and by the Consejería de Economía, Innovación, Ciencia y Empleo de la Junta de Andalucía (projects FQM-276, TIC-0130, P20_01160 and UHU-1260150).

Declaration of competing interest

The authors declare that they have no known competing financial interests or personal relationships that could have appeared to influence the work reported in this paper.

Acknowledgments

We thank the reviewers for their careful reading of the manuscript and their very constructive remarks, which have helped a lot to improve the presentation of the results.

Data availability

Data will be made available on request.

References

[1] Lorenz EN. Deterministic non-periodic flows. J Atmospheric. Sci 1963;20:130–41. http://dx.doi.org/10.1175/1520-0469(1963)020<0130:DNF>2.0.CO;2.
[2] Barrio R, Serrano S. Bounds for the chaotic region in the Lorenz model. Physica D 2009;238:1615–24. http://dx.doi.org/10.1016/j.physd.2009.04.019.
[3] Barrio R, Shilnikov A, Shilnikov L. Kneadings, symbolic dynamics and painting Lorenz chaos. Int J Bifurc Chaos. 2012;22:1230016. http://dx.doi.org/10.1142/S0218127412300169.
[4] Pelino V, Maimone F, Pasini A. Energy cycle for the Lorenz attractor. Chaos Solitons Fractals 2014;64:67–77. http://dx.doi.org/10.1016/j.chaos.2017.12.017.
[5] Munmuangsaen B, Srisuchinwong B. A hidden chaotic attractor in the classical Lorenz system. Chaos Solitons Fractals 2018;107:61–6. http://dx.doi.org/10.1016/j.chaos.2017.12.017.
[6] Li J, Yang Y. Similarity signature curves for forming periodic orbits in the Lorenz system. Chaos Solitons Fractals 2024;182:114751. http://dx.doi.org/10.1016/j.chaos.2024.114751.
[7] López AG, Benito F, Sabuco J, Delgado-Bonal A. The thermodynamic efficiency of the Lorenz system. Chaos Solitons Fractals 2023;172:113521. http://dx.doi.org/10.1016/j.chaos.2023.113521.
[8] Elgin JN, Molina Garza JB. Traveling wave solutions of the Maxwell–Bloch equations. Phys Rev A 1987;35:3986–8. http://dx.doi.org/10.1103/PhysRevA.35.3986.
[9] Knobloch E, Proctor MRE, Weiss NO. Heteroclinic bifurcations in a simple model of double-diffusive convection. J Fluid Mech 1992;239:273–92. http://dx.doi.org/10.1017/S0022112092004403.
[10] Algaba A, Domínguez-Moreno MC, Merino M, Rodríguez-Luis AJ. Study of the Hopf bifurcation in the Lorenz, Chen and Lü systems. Nonlinear Dynam 2015;79:885–902. http://dx.doi.org/10.1007/s11071-014-1709-2.
[11] Algaba A, Domínguez-Moreno MC, Merino M, Rodríguez-Luis AJ. Takens-Bogdanov bifurcations of equilibria and periodic orbits in the Lorenz system. Commun Nonlinear Sci Numer Simul 2016;30:328–43. http://dx.doi.org/10.1016/j.cnsns.2015.06.034.
[12] Llibre J, Messias M, da Silva PR. Global dynamics of the Lorenz system with invariant algebraic surfaces. Int J Bifurc Chaos 2010;20:3137–55. http://dx.doi.org/10.1142/S0218127410027593.
[13] Algaba A, Gamero E, Merino M, Rodríguez-Luis AJ. Resonances of periodic orbits in the Lorenz system. Nonlinear Dynam 2016;84:2111–36. http://dx.doi.org/10.1007/s11071-016-2632-5.
[14] Gonchenko S, Kazakov A, Turaev D, Shilnikov AL. Leonid shilnikov and mathematical theory of dynamical chaos. Chaos 2022;32:010402. http://dx.doi.org/10.1063/5.0080836.
[15] Champneys AR, Kuznetsov YA. Numerical detection and continuation of codimension–two homoclinic bifurcations. Int J Bifurc Chaos 1994;4:785–822. http://dx.doi.org/10.1142/S0218127494000587.
[16] Homburg AJ, Sandstede B. Homoclinic and heteroclinic bifurcations in vector fields. In: Broer H, et al., editors. Handbook of dynamical systems. vol. 3, Amsterdam: Elsevier; 2010, p. 379–524. http://dx.doi.org/10.1016/S1874-575X(10)00316-4.
[17] Guckenheimer J, Holmes P. Nonlinear oscillations, dynamical systems and bifurcations of vector fields, series on nonlinear science. vol. 42, New York: Springer; 1997, http://dx.doi.org/10.1007/978-1-4612-1140-2.
[18] Kuznetsov YA. Elements of applied bifurcation theory. New York: Springer; 2004, http://dx.doi.org/10.1007/978-3-031-22007-4.
[19] Wiggins S. Introduction to applied nonlinear dynamical systems and chaos. New York: Springer; 2003, http://dx.doi.org/10.1007/b97481.
[20] Bykov VV. The bifurcations of separatrix contours and chaos. Physica D 1993;62:290–9. http://dx.doi.org/10.1016/0167-2789(93)90288-C.
[21] Alfsen KH, Frøyland J. Systematics of the Lorenz model at $\sigma = 10$. Phys Scr 1985;31:15–20. http://dx.doi.org/10.1088/0031-8949/31/1/003.
[22] Glendinning P, Sparrow C. T-points: a codimension two heteroclinic bifurcation. J Stat Phys 1986;43:479–88. http://dx.doi.org/10.1007/BF01020649.
[23] Shil'nikov AL. On bifurcations of the Lorenz attractor in the Shimizu–Morioka model. Physica D 1993;62:338–46. http://dx.doi.org/10.1016/0167-2789(93)90292-9.

[24] Algaba A, Merino M, Freire E, Gamero E, Rodríguez-Luis AJ. Some results on Chua's equation near a triple-zero linear degeneracy. Int J Bifurc Chaos 2003;13:583–608. http://dx.doi.org/10.1142/S0218127403006741.
[25] Algaba A, Merino M, Rodríguez-Luis AJ. Homoclinic interactions near a triple-zero degeneracy in Chua's equation. Int J Bifurc Chaos 2012;22:1250129. http://dx.doi.org/10.1142/S0218127412501295.
[26] Rucklidge AM. Chaos in a low-order model of magnetoconvection. Physica D 1993;62:323–37. http://dx.doi.org/10.1016/0167-2789(93)90291-8.
[27] Rucklidge AM. Chaos in magnetoconvection. Nonlinearity 1994;7:1565–91. http://dx.doi.org/10.1088/0951-7715/7/6/003.
[28] Wieczorek S, Krauskopf B. Bifurcations of n-homoclinic orbits in optically injected lasers. Nonlinearity 2005;18:1095–120. http://dx.doi.org/10.1088/0951-7715/18/3/010.
[29] Fernández-Sánchez F, Freire E, Rodríguez-Luis AJ. T-points in a $\mathbb{Z}_2$-symmetric electronic oscillator. (I) Analysis. Nonlinear Dynam 2002;28:53–69. http://dx.doi.org/10.1023/A:1014917324652.
[30] Champneys AR, Rodríguez-Luis AJ. The non-transverse shil'nikov–Hopf bifurcation; uncoupling of homoclinic orbits and homoclinic tangencies. Physica D 1999;128:130–58. http://dx.doi.org/10.1016/S0167-2789(98)00311-X.
[31] Zimmermann MG, Natiello MA. Homoclinic and heteroclinic bifurcations close to a twisted heteroclinic cycle. Int J Bifurc Chaos 1998;8:359–75. http://dx.doi.org/10.1142/S0218127498000218.
[32] Homburg A, Natiello MA. Accumulations of T-points in a model for solitary pulses in an excitable reaction–diffusion medium. Physica D 2005;201:212–29. http://dx.doi.org/10.1016/j.physd.2004.12.007.
[33] Barrio R, Blesa F, Serrano S. Qualitative analysis of the rössler equations: bifurcations of limit cycles and chaotic attractors. Physica D 2009;238:1087–100. http://dx.doi.org/10.1016/j.physd.2009.03.010.
[34] Barrio R, Blesa F, Serrano S, Shilnikov A. Global organization of spiral structures in biparameter space of dissipative systems with Shilnikov saddle-foci. Phys Rev E 2011;84:035201. http://dx.doi.org/10.1103/PhysRevE.84.035201.
[35] Fernández-Sánchez F, Freire E, Rodríguez-Luis AJ. Analysis of the T-point-Hopf bifurcation. Physica D 2008;237:292–305. http://dx.doi.org/10.1016/j.physd.2007.09.002.
[36] Algaba A, Fernández-Sánchez F, Merino M, Rodríguez-Luis AJ. Analysis of the T-point-Hopf bifurcation with $\mathbb{Z}_2$-symmetry. Application to Chua's equation. Int J Bifurc Chaos 2010;20:979–93. http://dx.doi.org/10.1142/S0218127410026265.
[37] Algaba A, Fernández-Sánchez F, Merino M, Rodríguez-Luis AJ. Analysis of the T-point-Hopf bifurcation in the Lorenz system. Commun Nonlinear Sci Numer Simul 2015;22:676–91. http://dx.doi.org/10.1016/j.cnsns.2014.09.025.
[38] Labouriau IS, Rodrigues AAP. Global generic dynamics close to symmetry. J Differential Equations 2012;253:2527–57. http://dx.doi.org/10.1016/j.jde.2012.06.009.
[39] Rodrigues AAP. Repelling dynamics near a Bykov cycle. J Dyn Diff Eqs 2013;25:605–25. http://dx.doi.org/10.1007/s10884-013-9289-2.
[40] Rodrigues AAP, Labouriau IS. Spiralling dynamics near heteroclinic networks. Physica D 2014;268:34–49. http://dx.doi.org/10.1016/j.physd.2013.10.012.
[41] Doedel EJ, Champneys AR, Dercole F, Fairgrieve T, Kuznetsov Y, Oldeman BE, et al. Auto07-p: Continuation and bifurcation software for ordinary differential equations (with HomCont). Technical report, Concordia University; 2012.
[42] Algaba A, Merino M, Rodríguez-Luis AJ. Superluminal periodic orbits in the Lorenz system. Commun Nonlinear Sci Numer Simul 2016;39:220–32. http://dx.doi.org/10.1016/j.cnsns.2016.03.004.
[43] Fernández-Sánchez F, Freire E, Pizarro L, Rodríguez-Luis AJ. A model for the analysis of the dynamical consequences of a nontransversal intersection of the two-dimensional manifolds involved in a T-point. Phys Lett A 2003;320:169–79. http://dx.doi.org/10.1016/j.physleta.2003.11.011.
[44] Fernández-Sánchez F, Freire E, Rodríguez-Luis AJ. Bi-spiraling homoclinic curves around a T-point in Chua's equation. Int J Bifurcat. Chaos 2004;14:1789–93. http://dx.doi.org/10.1142/S0218127404010072.
[45] Belitskii GR. Functional equations and conjugacy of local diffeomorphisms of a finite smoothness class. Funktsional Anal I Prilozhen 1973;7(4):17–28; Funct Anal Appl 1973;7(4):268–77.
[46] Golmakani A, Homburg AJ. Lorenz attractors in unfoldings of homoclinic-flip bifurcations. Dyn Syst 2011;26:61–76. http://dx.doi.org/10.1080/14689367.2010.503186.
[47] Algaba A, Fernández-Sánchez F, Merino M, Rodríguez-Luis AJ. Homoclinic behavior around a degenerate heteroclinic cycle in a Lorenz-like system. Chaos Solitons Fractals 2024;186:115248. http://dx.doi.org/10.1016/j.chaos.2024.115248.
[48] Algaba A, Domínguez-Moreno MC, Merino M, Rodríguez-Luis AJ. A double-zero bifurcation in a Lorenz-like system. Nonlinear Dynam 2024;112:2305–30. http://dx.doi.org/10.1007/s11071-023-09130-1.
[49] Algaba A, Fernández-Sánchez F, Merino M, Rodríguez-Luis AJ. Chen's attractor exists if Lorenz repulsor exists: The Chen system is a special case of the Lorenz system. Chaos 2013;23:033108. http://dx.doi.org/10.1063/1.4813227.
[50] Algaba A, Fernández-Sánchez F, Merino M, Rodríguez-Luis AJ. The Lü system is a particular case of the Lorenz system. Phys Lett A 2013;377:2771–6. http://dx.doi.org/10.1016/j.physleta.2013.08.034.